Atmos. Chem. Phys., 15, 7913–7927, 2015
www.atmos-chem-phys.net/15/7913/2015/
doi:10.5194/acp-15-7913-2015

Atmospheric Chemistry and Physics
Open Access

The impact of parameterising light penetration into snow on the photochemical production of NO_x and OH radicals in snow

H. G. Chan[1,2], **M. D. King**[2], **and M. M. Frey**[1]

[1]British Antarctic Survey, Natural Environment Research Council, Cambridge, CB3 0ET, UK
[2]Department of Earth Sciences, Royal Holloway University of London, Egham, Surrey, TW20 0EX, UK

Correspondence to: H. G. Chan (hohan47@bas.ac.uk)

Received: 21 January 2015 – Published in Atmos. Chem. Phys. Discuss.: 23 March 2015
Revised: 23 June 2015 – Accepted: 3 July 2015 – Published: 17 July 2015

Abstract. Snow photochemical processes drive production of chemical trace gases in snowpacks, including nitrogen oxides ($NO_x = NO + NO_2$) and hydrogen oxide radical ($HO_x = OH + HO_2$), which are then released to the lower atmosphere. Coupled atmosphere–snow modelling of theses processes on global scales requires simple parameterisations of actinic flux in snow to reduce computational cost. The disagreement between a physical radiative-transfer (RT) method and a parameterisation based upon the *e*-folding depth of actinic flux in snow is evaluated. In particular, the photolysis of the nitrate anion (NO_3^-), the nitrite anion (NO_2^-) and hydrogen peroxide (H_2O_2) in snow and nitrogen dioxide (NO_2) in the snowpack interstitial air are considered.

The emission flux from the snowpack is estimated as the product of the depth-integrated photolysis rate coefficient, υ, and the concentration of photolysis precursors in the snow. The depth-integrated photolysis rate coefficient is calculated (a) explicitly with an RT model (TUV), υ_{TUV}, and (b) with a simple parameterisation based on *e*-folding depth, υ_{z_e}. The metric for the evaluation is based upon the deviation of the ratio of the depth-integrated photolysis rate coefficient determined by the two methods, $\frac{\upsilon_{\mathrm{TUV}}}{\upsilon_{z_e}}$, from unity. The ratio depends primarily on the position of the peak in the photolysis action spectrum of chemical species, solar zenith angle and physical properties of the snowpack, i.e. strong dependence on the light-scattering cross section and the mass ratio of light-absorbing impurity (i.e. black carbon and HULIS) with a weak dependence on density. For the photolysis of NO_2, the NO_2^- anion, the NO_3^- anion and H_2O_2 the ratio $\frac{\upsilon_{\mathrm{TUV}}}{\upsilon_{z_e}}$ varies within the range of 0.82–1.35, 0.88–1.28, 0.93–1.27 and 0.91–1.28 respectively. The *e*-folding depth parameterisation underestimates for small solar zenith angles and overestimates at solar zenith angles around 60° compared to the RT method. A simple algorithm has been developed to improve the parameterisation which reduces the ratio $\frac{\upsilon_{\mathrm{TUV}}}{\upsilon_{z_e}}$ to 0.97–1.02, 0.99–1.02, 0.99–1.03 and 0.98–1.06 for photolysis of NO_2, the NO_2^- anion, the NO_3^- anion and H_2O_2 respectively. The *e*-folding depth parameterisation may give acceptable results for the photolysis of the NO_3^- anion and H_2O_2 in cold polar snow with large solar zenith angles, but it can be improved by a correction based on solar zenith angle and for cloudy skies.

1 Introduction

Field and laboratory experiments over the past 2 decades have provided evidence that photochemical reactions occurring within snow lead to the emission of various gaseous compounds from the snowpack (e.g. Jacobi et al., 2004; Jones et al., 2000; Beine et al., 2002, 2006; Dibb et al., 2002; Simpson et al., 2002) and production of radicals, e.g. hydroxyl radical (OH), within the snowpack (e.g. Mauldin et al., 2001; Chen et al., 2004; Sjostedt et al., 2005; France et al., 2011). The porous structure of snowpacks allows the exchange of gases and particles with the atmosphere. The exchange between snowpack and overlying atmosphere depends on dry and wet deposition, transport (including wind pumping and diffusion) and snow microphysics (e.g. Bartels-Rausch et al., 2014). Thus snow can act as both a source and a sink of atmospheric chemical species as summarised in Bartels-Rausch et al. (2014) and Grannas et al. (2007). Photochemistry in the snowpack needs to be fully understood because (1) emitted photolysis products play an impor-

tant role in determining the oxidising capacity of the lower atmosphere – e.g. concentration of O_3, HO_x, H_2O_2 – and (2) chemical preserved in ice cores, and potential palaeoclimate proxies, may be altered by reactions with OH radicals, photolysis or physical uptake and release (Wolff and Bales, 1996).

The photolytic lifetime of a chemical species in the snowpack is the reciprocal of the photolysis rate coefficient (also known as the photodissociation rate coefficient), J, which is dependent on the actinic flux (also known as spherical or point irradiance) in the snowpack, I, the quantum yield of the photolysis reaction, Φ, and absorption cross section of the photolysing species, σ.

$$J(\theta, z, T) = \int \sigma(\lambda, T)\, \Phi(\lambda, T)\, I(\theta, z, \lambda)\, \mathrm{d}\lambda, \quad (1)$$

where θ is solar zenith angle, z is the depth into the snowpack, λ is the wavelength of the incident solar radiation and T is the temperature of the snowpack.

Under clear-sky conditions, a homogeneous snowpack can be separated into two optical layers based on the propagation of actinic flux from the surface into the snow: the near-surface layer, i.e. the top few centimetres of the snowpack, where direct solar radiation is converted into diffuse radiation. Below the near-surface layer is the asymptotic zone, where all solar radiation is diffuse and will decrease exponentially with depth (Warren, 1982).

The relationship between actinic flux (and the photolysis rate coefficient) and depth is complex near the surface of the snowpack due to rapidly changing contributions from both direct and diffuse radiation. Enhancement or attenuation of actinic flux in the near-surface layer compared to above the snow is dependent on the solar zenith angle (Fig. 1 and Fig. 4 in Lee-Taylor and Madronich, 2002). Snowpack is a very scattering and low absorption environment for UV–visible photons with individual snow grains tending to forward-scatter photons (Warren, 1982). The enhancement in actinic flux compared to above the snow occurs for solar zenith angles $< 50°$. For solar zenith angles $\sim 50°$ actinic flux will decrease almost exponentially with depth (Wiscombe and Warren, 1980). For direct radiation from a low sun (large solar zenith angle, i.e. $> 50°$) there is a larger probability that the photons will be scattered upwards and out of the snowpack, leading to a rapid decrease in actinic flux with depth in the first few centimetres of the snowpack, i.e. decreasing faster than exponential (Warren, 1982).

In the asymptotic zone radiation is diffused, and provided that the snowpack is semi-infinite – i.e. the albedo of the surface underlying the snow does not affect the calculation of the actinic flux within the snowpack – the radiation decreases exponentially according to Beer–Lambert law (France et al., 2011, define semi-infinite as 3–4 e-folding depths).

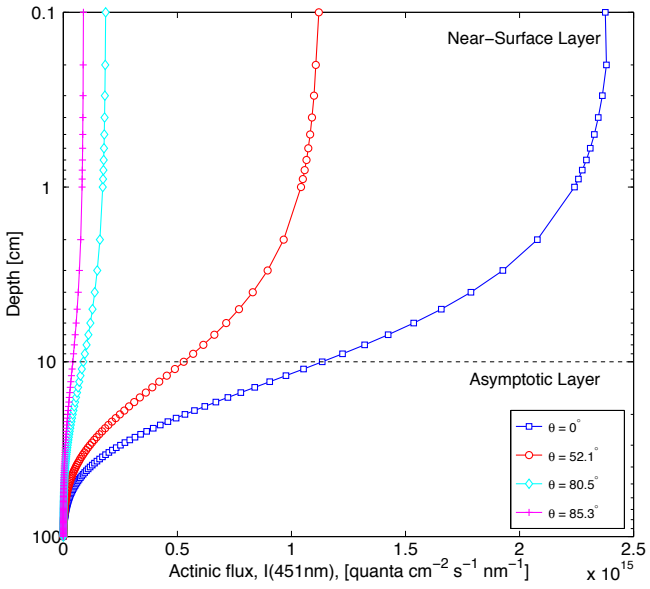

Figure 1. Depth profile within "cold polar snow" (base case: $\rho = 0.4\,\mathrm{g\,cm^{-3}}$, $[\mathrm{BC}] = 4\,\mathrm{ng(C)\,g^{-1}}$ and $\sigma_{\mathrm{scatt}} = 25\,\mathrm{m^2\,kg^{-1}}$) of actinic flux, I, at $\lambda = 451$ nm at different solar zenith angles θ.

$$I(z, \lambda) = I_0\, e^{-\frac{z - z_0}{z_e(\lambda)}}, \quad (2)$$

where I_0 is the actinic flux at a reference depth z_0 within the asymptotic zone, and $z_e(\lambda)$ is the asymptotic e-folding depth at which I has decayed to $1/e$, $\sim 37\,\%$ of its reference value, I_0.

Radiative-transfer (RT) models, such as the TUV-snow model (Lee-Taylor and Madronich, 2002), were developed to capture the non-exponential attenuation of radiation near the surface of the snowpack. However, running a radiative-transfer model is a time-consuming step within large-scale (e.g. 3-D) chemical transport models or global climate models, so photolysis rate coefficients in the snowpack, J, are often parameterised with e-folding depth (e.g. Thomas et al., 2011), i.e.

$$J_{z_e}(\theta, z) = J_0(\theta)\, e^{-\frac{z - z_0}{z_e(\lambda)}}, \quad (3)$$

where $J_{z_e}(\theta, z)$ is the parameterised photolysis rate coefficient at depth z; J_0 is the photolysis rate coefficient at the surface of the snowpack at solar zenith angle θ; and z_e is the e-folding depth of the snowpack. The aim of this paper is to investigate the accuracy of the e-folding depth parameterisation (Eq. 3) relative to a value of J calculated using a physically explicit RT model and Eq. (1). The metric to compare the two models is the depth-integrated photolysis rate coefficient (also known as the transfer velocity; France et al., 2007), which may be considered approximately proportional to the flux of potential gaseous photo-produced compounds

Table 1. Reference for quantum yield, Φ, used for Reactions (R1)–(R4) and (R7) and absorption cross section, σ, of the NO_3^- anion, the NO_2^- anion, H_2O_2, and NO_2.

Reaction	Reference for Φ	Quantum yield, Φ at 258 K	Action spectrum peak $\lambda_{\text{act peak}}$, nm
R1	Chu and Anastasio (2003)	0.00338	321
R2	Warneck and Wurzinger (1988)	0.00110	321
R3	Chu and Anastasio (2007)	0.12066*	345
R4	Gardner et al. (1987)	0.97900	375
R7	Chu and Anastasio (2005)	0.68300	321
Species	Reference for σ		
NO_3^-	Chu and Anastasio (2003)		
NO_2^-	Chu and Anastasio (2007)		
NO_2	DeMore et al. (1997)		
H_2O_2	Chu and Anastasio (2005)		

* Quantum yield at $\lambda = 345$ nm, the photochemical action spectrum peak of the NO_2^- anion.

from the snowpack. The depth-integrated photolysis rate coefficient, v, is calculated (Simpson et al., 2002) as

$$v(\theta) = \int J(\theta, z)\,\mathrm{d}z. \tag{4}$$

The depth-integrated production rate of a chemical species B from the photolysis of a chemical species A, $F_B(\theta)$, is the product of concentration of A, $[A]$, and the depth-integrated photolysis rate coefficient, v_A, assuming the concentration of A is constant with depth.

$$F_B(\theta) = [A]\, v_A(\theta) \tag{5}$$

For example, the photolysis of the nitrate anion, NO_3^-, is important and has therefore been studied extensively in the past. It leads to emission of nitrogen oxides ($NO_x = NO + NO_2$) to the atmosphere. The following reactions summarise the main channels of NO_x production from NO_3^- photolysis in snowpack. The quantum yield and absorption cross section of all the chemical species used in this study are listed in Table 1.

$$NO_3^- + h\nu \rightarrow NO_2 + O^-, \quad \lambda_{\text{act peak}} = 321\,\text{nm}, \tag{R1}$$

$$NO_3^- + h\nu \rightarrow NO_2^- + O(^3P), \quad \lambda_{\text{act peak}} = 321\,\text{nm}, \tag{R2}$$

$$NO_2^- + h\nu \rightarrow NO + O^-, \quad \lambda_{\text{act peak}} = 345\,\text{nm}, \tag{R3}$$

where $h\nu$ represents a photon and $\lambda_{\text{act peak}}$ is the wavelength corresponding to the maximum in the action spectrum. Here the action spectrum is the spectral photolysis rate coefficient plotted as a function of wavelength. For example, the action spectrum shows that nitrate photolysis is most efficient at 321 nm. Snow is a porous medium in which gas-phase reactions can occur in the interstitial air. Gaseous nitrogen dioxide (NO_2) has a large quantum yield, and its action spectrum peak is in the UV-A wavelengths, around 375 nm. Long-wavelength UV light penetrates deeper into the snowpack than shorter-wavelength UV. Therefore, NO_2 photolyses within the snowpack and may produce ozone (Reactions R4 and R5).

$$NO_2 + h\nu \rightarrow NO + O(^3P), \quad \lambda_{\text{act peak}} = 375\,\text{nm}, \tag{R4}$$

$$O(^3P) + O_2 + M \rightarrow O_3 + M \tag{R5}$$

Studies have also demonstrated that photolysis of NO_3^- and NO_2^- in snow and ice contribute to the formation of OH radicals within the snowpack (Dubowski et al., 2001, 2002; Cotter et al., 2003; Chu and Anastasio, 2003; Anastasio and Chu, 2008) through reaction of oxygen radical anion (O^-) with water (Reaction R6).

$$O^- + H_2O \rightarrow OH + OH^- \tag{R6}$$

In the presence of oxygen, formation of the OH radical may create a radical-initiated oxidising medium allowing oxidation of organic chemicals to emit species such as formaldehyde, acetaldehyde or organic halogens to the lower atmosphere (McNeill et al., 2012). Another source of OH radicals in the snowpack is photolysis of hydrogen peroxide (H_2O_2) (Chu and Anastasio, 2005, 2007):

$$H_2O_2 + h\nu \rightarrow 2OH, \quad \lambda_{\text{act peak}} = 321\,\text{nm}. \tag{R7}$$

The ratio of the depth-integrated photolysis rate coefficients, $Q = \frac{v_{\text{TUV}}}{v_{z_e}}$, determined from the two methods – the RT model and e-folding depth parameterisation – were calculated for the photolysis of NO_3^-, NO_2^-, NO_2 and H_2O_2 in snow. Reactions rate coefficients for Reactions (R1)–(R4) and (R7) were determined for hypothetical snowpacks with different physical and optical properties and under different environmental conditions, e.g. total column ozone.

2 Modelling procedure

The hypothetical homogeneous snowpacks defined in this study were based on three different types of snow – cold polar, wind-packed and melting snow (Table 2, Marks and King, 2014). The snowpacks are assumed to be semi-infinite.

Sensitivity tests calculating Q were run against the following parameters – base case: a typical cold polar snowpack; case 1: the density of the snowpack was varied; case 2: the scattering cross section was varied; case 3: the black carbon (BC) mass ratio was varied; case 4: the HUmid LIke Substances (HULIS) mass ratio was varied; case 5: the mass ratio with both BC and HULIS was varied; case 6: the asymmetry factor was varied; and case 7: the total column ozone was varied. Values for these parameters, listed in Table 3, were chosen based on previous field measurements made in various geographic locations and conditions (i.e. Grenfell et al., 1994; Beaglehole et al., 1998; King and Simpson, 2001; Fisher et al., 2005; France et al., 2010; Marks and King, 2014).

In case 1, snow densities were varied in the range observed typically in natural snowpack of 0.2–0.6 $\mathrm{g\,cm^{-3}}$ (Marks and King, 2014, and references therein).

In cases 2–5, the scattering cross section and mass ratio of light-absorbing impurities of the snowpack were varied – both of which have an impact on the propagation of actinic flux within the snowpack. The reciprocal of the e-folding depth, z_e, is the asymptotic flux extinction coefficient, κ_{ext}, which is the sum of the scattering, r_{scatt}, and absorption coefficients, μ (Lee-Taylor and Madronich, 2002). The scattering and absorption coefficients describe the attenuation per unit length, and both are density-dependent (Lee-Taylor and Madronich, 2002). For general use, the following scattering, σ_{scatt}, and absorption, σ_{abs}, cross sections are introduced:

$$\sigma_{\mathrm{ext}} = \sigma_{\mathrm{scatt}} + \sigma_{\mathrm{abs}}, \tag{6}$$

where $\sigma_{\mathrm{ext}} = \kappa_{\mathrm{ext}}/\rho$ is the extinction cross section, $\sigma_{\mathrm{scatt}} = r_{\mathrm{scatt}}/\rho$ is the scattering cross section of snow and $\sigma_{\mathrm{abs}} = \mu/\rho$ is the absorption cross section of snow and light-absorbing impurities. In case 2, values of σ_{scatt} were selected to cover a wide range of snow types (Table 2). The values of the scattering cross section are assumed to be independent of wavelength (Lee-Taylor and Madronich, 2002).

The absorption cross section of snowpack is due to wavelength-dependent absorption by ice, $\sigma_{\mathrm{abs}}^{\mathrm{ice}}$, and light-absorbing impurities, σ^{+}, such as black carbon and HULIS:

$$\sigma_{\mathrm{abs}} = \sigma_{\mathrm{abs}}^{\mathrm{ice}} + \sigma^{+}. \tag{7}$$

Warren et al. (2006) showed that BC can dominate the absorption in snow as it is a factor of ~ 50 more efficient absorber of light than mineral dust particles of the same mass. Thus in sensitivity test case 3, black carbon is considered to be the only light-absorbing impurity. For the work presented here the light-absorption cross section of black carbon, σ_{BC}^{+}, is assumed to be wavelength-independent and equal to $\sim 10\,\mathrm{m^2\,g^{-1}}$ (France et al., 2010; Lee-Taylor and Madronich, 2002). To account for all pollution scenarios, from clean to dirty, the mass ratio of black carbon is varied from 4 to 128 $\mathrm{ng\,g^{-1}}$, to cover the concentration range typically measured in coastal (Beaglehole et al., 1998), Antarctica-near research stations (Zatko et al., 2013) or in midlatitude snow. Other common pollutants found in snow samples include HULIS, which represent an important fraction of biomass burning, biogenic and marine aerosol etc. (e.g. Voisin et al., 2012). HULIS absorb most effectively in the UV region of the solar spectrum, and the absorption cross section decreases towards the visible (Hoffer et al., 2006). Concentrations of HULIS measured in polar snow vary between 1 and 1000 $\mathrm{ng\,g^{-1}}$ and depend on the measurement method (Voisin et al., 2012; France et al., 2012), which is taken into account by the range of values used in case 4. In natural snow, it is rare that HULIS would be the only light-absorbing impurity within snow as shown in France et al. (2011) and France and King (2012); therefore, in case 5 a combination of both black carbon and HULIS were used and varied.

In case 6, the asymmetry factor, g, is the average cosine of the scattering angle and is a measure of the preferred scattering direction. Sensitivity tests were run with two different values of g of 0.89 and 0.86 as discussed by Marks and King (2014) and Libois et al. (2014) respectively. Both selected values are close to 1, indicating light scattering by snow grains is dominated by forward scattering.

Within case 7, column ozone values were varied to cover the seasonal and spatial variability observed above the polar regions. The effect of column ozone on the depth-integrated photolysis rate coefficient ratio was explored as downwelling UV radiation is very sensitive to stratospheric ozone absorption and the attenuation is a strong function of wavelength. Typical value of column ozone in Antarctica (also the global average; Kroon et al., 2008) is about 300 DU but can be as low as 150 DU in the Antarctic O_3 hole (Kramarova et al., 2014). Column ozone generally increases from the tropics to midlatitudes. Therefore, there are three different values of total column ozone: 200, 300 and 400 DU.

Table 2. Properties of snow type studied. Optical and physical properties are based on work by Marks and King (2014) and references therein.

Snow type	ρ $\mathrm{g\,cm^{-3}}$	σ_{scatt} $\mathrm{cm^2\,kg^{-1}}$
Cold polar snow	0.2–0.6	15–25
Wind-packed snow	0.2–0.6	5–10
Melting snow	0.2–0.6	0.2–2

Table 3. Optical properties of the snowpacks used. The bold numbers are to highlight the optical property that is varying in that particular case.

	ρ $g\,cm^{-3}$	[BC] $ng(C)\,g^{-1}$	σ_{scatt} $m^2\,kg^{-1}$	O_3 col. DU	g	z_e * cm^{-1}	Designation
Base case	0.4	4.0	25	300	0.89	13.3	BaseC
Case 1	**0.2**	4.0	25	300	0.89	25.2	Den0.2
Density of snowpack	**0.6**	4.0	25	300	0.89	9.1	Den0.6
Case 2	0.4	4.0	**2**	300	0.89	35.3	Scatt2
Scattering cross section	0.4	4.0	**7**	300	0.89	24.4	Scatt7
Case 3	0.4	**0.18**	25	300	0.89	36.9	BC0.18
Black carbon content	0.4	**32.0**	25	300	0.89	4.9	BC32
	0.4	**128.0**	25	300	0.89	2.5	BC128
Case 6, g	0.4	4.0	25	300	**0.86**	12.0	g0.86
Case 7	0.4	4.0	25	**200**	0.89	13.3	$O_3$200
Ozone column	0.4	4.0	25	**400**	0.89	13.3	$O_3$400
	ρ $g\,cm^{-3}$	[HULIS] $ng\,g^{-1}$	σ_{scatt} $m^2\,kg^{-1}$	O_3 col. DU	g	z_e * cm^{-1}	Designation
Case 4	0.4	**1.0**	25	300	0.89	36.9	HULIS1
HULIS content	0.4	**8.0**	25	300	0.89	22.0	HULIS8
	0.4	**17.0**	25	300	0.89	15.3	HULIS17
	0.4	**1000.0**	25	300	0.89	2.06	HU1000
	0.4	**17.0**	**2**	300	0.89	37.0	HU17S2
	0.4	**1000.0**	**2**	300	0.89	7.3	HU1000S2
Case 5		[BC] + [HULIS]					
Combined	0.4	**0.6 + 8**	**7**	300	0.89	30.6	Comb

* For cases 1–2 and 4–6, the reported e-folding depth, z_e, is the average of e-folding depth at 321, 345 and 375 nm. For cases 3 and 7, z_e is the e-folding depth at 321 nm

2.1 RT method: radiative-transfer model, TUV

The attenuation of actinic flux with depth was calculated by a coupled atmosphere–snow radiative-transfer model, TUV 4.4, using an eight-stream DISORT (Discrete Ordinates Radiative Transfer Program for a Multi-Layered Plane-Parallel Medium) model (Lee-Taylor and Madronich, 2002). The model treats the snow as a weakly absorbing, very scattering homogenous layer with its optical properties described by the variables g, σ_{scatt}, and σ_{abs}. The snowpacks were modelled as described in detail in Lee-Taylor and Madronich (2002) except the absorption cross section of ice was updated to values given by Warren and Brandt (2008). The model configuration in this study used 110 snowpack layers with 1 mm spacing in the top 1 cm and 1 cm spacing for the rest of the 1 m snowpack, and 72 atmospheric layers with 1 m spacing for the first 10 m above snowpack surface then 10 m intervals until 100 m, 100 m interval up to 1 km, 1 km intervals up to 10 km and 2 km intervals up to 80 km, with no atmospheric loading of aerosol and assumed clear-sky conditions.

Values of the photolysis rate coefficient, J, for Reactions (R1)–(R4) and (R7) were calculated by TUV using Eq. (1). The absorption cross section of the chromophores in the ice phase are assumed to be the same as the aqueous phase and are listed with temperature-dependent quantum yields for reactions used in this study (Table 1). Photolysis rate coefficients calculated with the TUV are referred to as the "RT method".

2.2 z_e method: e-folding depth

The e-folding depths, z_e, for the snowpacks described in Table 3 were calculated by fitting Eq. (2) to an actinic flux depth profile through snowpack obtained from TUV with a vertical resolution of 1 cm from 20 cm below the snowpack surface. At this depth, radiation is effectively diffuse and decays exponentially with depth (asymptotic zone). Field measurements of e-folding depth have been previously carried out over similar depths in the snowpack (e.g. France and King, 2012).

Values of z_e were determined for three wavelengths (λ = 321, 345 and 375 nm) and at seven different solar zenith angles (0, 36.9, 53.1, 66.4, 78.5, 80 and 90°). These wavelengths were chosen as they represent the peak of the pho-

tolysis action spectrum for each chemical species (Table 1). The photolysis rate coefficients were approximated by scaling the surface photolysis rate coefficient calculated by the RT method (TUV model) with the average e-folding depth, z_e, over seven solar zenith angles at a wavelength that is near the peak of the action spectrum of the chemical species (as shown in Eq. 3). For example in the case of NO_3^- photolysis,

$$J_{z_e,NO_3^-}(\theta,z) = J_{NO_3^-}(\theta,z_0)\, e^{-\frac{z-z_0}{z_e(\lambda=321\,\mathrm{nm})}}, \quad (8)$$

where $J_{z_e,NO_3^-}(\theta,z)$ is the parameterised photolysis rate coefficient at depth z; $J_{NO_3^-}(\theta,z_0)$ is the photolysis rate coefficient of NO_3^- at the surface obtained by the RT method (TUV model); and $z_e^{\lambda=321\,\mathrm{nm}}$ is the e-folding depth, z_e, at a wavelength of 321 nm. For clarity, this e-folding depth parameterisation is called the "z_e method".

2.3 Ratio of depth-integrated photolysis rate coefficients

To determinate the accuracy of the z_e method relative to the RT method, the ratio of depth-integrated photolysis rate coefficients, Q, was determined. The Q ratio is defined as depth-integrated photolysis rate coefficient calculated with the RT method over the depth-integrated photolysis rate coefficients estimated by the z_e method. For example, Q in the case of NO_2 (Reaction R1) is given by

$$Q = \frac{v_{TUV,NO_2}}{v_{z_e,NO_2}} = \frac{\int J_{NO_3^-\rightarrow NO_2}(z)\,\mathrm{d}z}{J_{NO_3^-\rightarrow NO_2}(z_0)\int e^{-\frac{z-z_0}{z_e^{\lambda=321\,\mathrm{nm}}}}\,\mathrm{d}z}, \quad (9)$$

where $J_{z_e,NO_3^-\rightarrow NO_2}(z_0)$ is the photolysis rate coefficient for NO_3^- photolysis at the surface of the snowpack. For Reactions (R3), (R4) and (R7), the surface photolysis rate coefficients were scaled, with $e^{\frac{-z-z_0}{z_e}}$ with e-folding depth at 345, 375 and 321 nm respectively for each depth z.

3 Results and discussion

The study evaluates the accuracy of parameterisation of photolysis rate coefficient to variation in solar zenith angle, different photolysis precursors, snowpack properties and total column ozone. Correction factors were also found for each different species to improve the performance of the z_e method.

3.1 The response of e-folding depth to solar zenith angle and wavelength

Radiation in the asymptotic layer, i.e. below the first few centimetres of the snow surface (Fig. 1), decreases exponentially with depth as observed previously at various polar and non-polar sites (Warren and Wiscombe, 1980; Marks and King, 2014; Fisher et al., 2005; King and Simpson, 2001). Table 3 lists the average e-folding depth across seven solar zenith angles for all cases. For the base case, cases 1–3, 6 and 7, the e-folding depths listed are averaged not only across solar zenith angles but also across three wavelengths (321, 345 and 375 nm). There are no significant differences between the calculated e-folding depths, across different solar zenith angles or across the three wavelengths of which the variation coefficients are between 0.002 and 2 %. For snowpacks in cases 4 and 5, the e-folding depths were at a single wavelength (321 nm) only and the variation coefficients range from 0.007 to 0.16 %. Figure 2 shows how e-folding depth varies with wavelength and density, black carbon mass ratio, HULIS mass ratio or scattering cross section of the snowpack. At all wavelengths, the e-folding depth decreases with increasing snow density, and increasing the mass ratio of the black carbon increased the absorption of incident radiation. Absorption of HULIS is wavelength-dependent; i.e. increasing mass ratio of HULIS only increases absorption of UV and near-UV radiation. However, the absorption of the incident radiation in the visible wavelengths is independent of the mass ratio of HULIS. Increasing the scattering cross section also leads to a decrease in e-folding depth.

Scattering of photons typically occurs at the air–ice interface of a snow grain and absorption occurs within the snow grain. A denser snowpack implies more scattering or absorp-

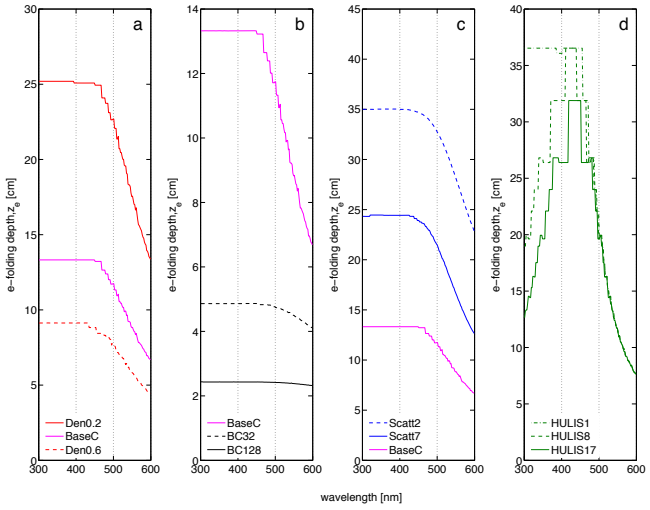

Figure 2. The e-folding depth, z_e, as a function of wavelength and dependence on **(a)** snow density, ρ (case 1); **(b)** scattering cross section, σ_{scatt} (case 2); **(c)** absorption due to black carbon, [BC] (case 3); **(d)** absorption due to HULIS, [HULIS] (case 4). Values of e-folding depth decrease as values of density, black carbon mass ratio and scattering cross section increase across wavelengths between 300 and 600 nm. For snowpacks containing black carbon as the only absorber other than ice, the change in e-folding depths are not sensitive to wavelength in the UV and near UV. However, for snowpacks containing e.g. HULIS the change in e-folding depth is sensitive to wavelength.

tion events per unit length. A larger scattering cross section will typically reduce the path length of a photon through the snowpack and reduce the possibility for absorption by ice or light-absorbing impurities. Therefore, increases in density, light-absorbing impurities and scattering cross section result in a smaller e-folding depth.

3.2 Variation of Q, ratio of depth-integrated photolysis rate coefficients

Depth-integrated photolysis rate coefficients of the four chemical species considered (NO_3^-, NO_2^-, H_2O_2 and NO_2) were calculated by the RT method and the z_e method. To evaluate the accuracy of the approximation by the z_e method, the ratio Q ($\frac{v_{TUV}}{v_{ze}}$ using Eq. 9), is calculated and considered independently.

3.2.1 Variation with solar zenith angle

When the solar zenith angle is between 0 and 37°, using the z_e method leads to a depth-integrated photolysis rate coefficient ratio, Q, of up to 1.35 (Fig. 3). The underestimation of the z_e method at small solar zenith angles is due to the enhancement of actinic flux compared to above the surface in the near-surface layer being considered in the RT method but being neglected in the z_e method. For solar zenith angles around 50° and larger than 80° the value of Q is close to unity, suggesting the z_e method may be a good approximation for these solar zenith angles. Wiscombe and Warren (1980) suggested that solar illumination around a solar zenith angle of 50° was effectively the same as diffuse radiation, which deceases exponentially with depth from the snow surface. At large solar zenith angles (> 80°) there is little direct solar radiation relative to diffuse radiation illuminating the snowpack and the snowpack is effectively illuminated by diffuse radiation; thus the difference between the two methods is small. Between the solar zenith angles of ∼66 and 75°, i.e. minimum values of Q in Fig. 3, the direct radiation entering the snowpack may be potentially scattered out of the snowpack due to the strong forward-scattering property of snow. Hence, the actinic flux attenuates at a quicker rate than the e-folding depth in the near-surface zone, and the z_e method overestimates the intensity of solar radiation in the snowpack.

In reality, only high-altitude glaciers in the tropics, such as those found in the Himalayas or Andes, would experience the overhead sun or small solar zenith angles in the summer. In the polar regions, where snow emission can dominate boundary layer chemistry (e.g. Davis et al., 2004), solar zenith angles vary between 42.8° (Antarctic/Arctic Circle) and 66.5° (at the pole) at summer solstice and close to or greater than 90° during winter solstice for the Antarctic/Arctic Circle. Within this solar zenith angle range, the z_e method is most likely to yield small overestimates of fluxes and photochemical production rate. However, small "effective" solar zenith angles can be achieved in sloping snow-covered terrain, as shown in Fig. 4. The effective solar zenith angle, θ_{eff}, on a snow-covered slope is the difference between the solar zenith angle normal to a horizontal surface, θ_{dir}, and the angle of the slope, ϕ. Therefore, the z_e method might lead to underestimation of depth-integrated production rates on snow-covered mountains.

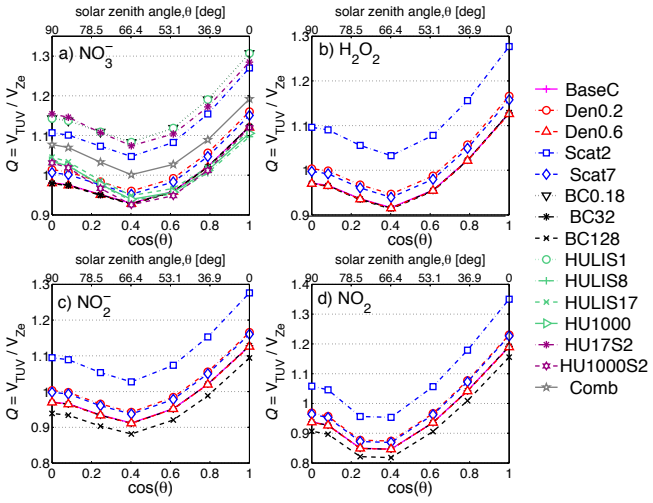

Figure 3. The ratio of depth-integrated photolysis rate coefficient, $Q = \frac{v_{TUV}}{v_{ze}}$, for the two different methods as a function of solar zenith angle, θ. **(a)** NO_3^- anion; **(b)** H_2O_2; **(c)** NO_2^- anion; **(d)** NO_2. Magenta: BaseC snowpack ($\rho = 0.4\,g\,cm^{-3}$, $[BC] = 4\,ng(C)\,g^{-1}$ and $\sigma_{scatt} = 25\,m^2\,kg^{-1}$).

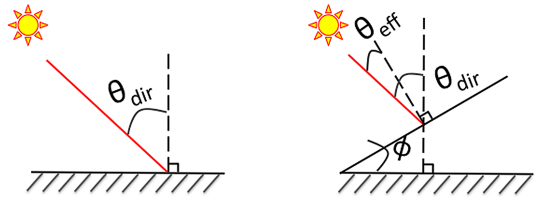

Figure 4. The effective solar zenith angle, θ_{eff}, is the same as the solar zenith angle of direct solar radiation, θ_{dir}, on a flat surface (left). However, on a surface that has an incline (right) the effective solar angle, θ_{eff}, is the difference of the direct solar zenith angle and the angle of the surface, ϕ, and typically smaller.

3.2.2 Variation with chemical species and total column ozone

The value of the ratio Q for the photolysis of the NO_3^- anion and H_2O_2 is very similar in terms of its response to changing solar zenith angle (Fig. 3a and b). The maximum and minimum values of Q are ∼1.27 (underestimation of solar radiation by the z_e method), at direct overhead sun, and ∼0.92 (overestimation of solar radiation by the z_e method), at solar zenith angles of ∼66–70°. The disagreement between the two methods for the photolysis of NO_2^- is slightly larger,

with the ratio Q ranging between 0.88–1.28 (Fig. 3c). The approximation with the z_e method is the most inaccurate for the photolysis of NO_2 within snowpack interstitial air, having Q values range between 0.82 and 1.35 (Fig. 3d).

The NO_3^- anion and H_2O_2 have the peak of their action spectrum in the UV-B, while the NO_2^- anion and NO_2 have a peak in near-UV and visible wavelengths respectively. Solar radiation in the UV region is less intense and more diffuse relative to the UV-A and visible radiation at the snow surface as (1) the ozone layer absorbs strongly in the UV-B and UV-C while relatively weakly in the UV-A and almost negligibly in the visible region and (2) the Rayleigh scattering of photons by air molecules increases as the wavelength decreases. The actinic flux attenuation profile with depth, in snow, of more diffused actinic flux can be better approximated by the e-folding depth; therefore, the z_e method provides a better estimation of photolysis rate coefficient profile for NO_3^- and H_2O_2 compared to NO_2^- and NO_2.

The wavelength of the peak in the action spectrum of a chemical species also has an impact on its response to changes in column ozone concentration (case 7) in terms of photolysis rate coefficient. The surface photolysis rate coefficients for NO_3^- and H_2O_2 are more sensitive to the changes in column ozone, due to their action spectrum peak in the UV-B region, compared to species that have their peak in UV-A, such as NO_2^- and NO_2. The surface values of $J_{NO_3^-}$ (Fig. 5a) and $J_{H_2O_2}$ increased by $\sim 20\,\%$ when total ozone column decreased from 300 to 200 DU, while surface values of $J_{NO_2^-}$ and J_{NO_2} (Fig. 5b) only increased by approximately 6 and 0.9 % respectively. When total ozone column increased from 300 to 400 DU, surface values of $J_{NO_3^-}$ and $J_{H_2O_2}$ dropped approximately by $\sim 14\,\%$, whereas surface values of $J_{NO_2^-}$ and J_{NO_2} only decreased by ~ 5 and 0.6 % respectively.

Despite the value of the photolysis rate coefficient varying with values of different column ozone, especially for the NO_3^- anion and H_2O_2, the propagation of radiation throughout the snowpack was not affected by the column ozone; i.e. the value of Q was unchanged by changing the ozone column, and the z_e method is not sensitive to ozone column values.

3.2.3 Variation with snow physical properties

Density (case 1), scattering cross section (case 2), light-absorbing impurities (cases 3–5) and asymmetry factor (case 6) were considered as the four varying physical properties of the snowpack in this study. Figure 3 highlights three results in terms of various physical properties of the snowpacks: Firstly, snow density has a small effect on the ability of the z_e method to reproduce the results of RT method. Secondly, the z_e method underestimates depth-integrated photolysis rate coefficients significantly for relatively clean snowpacks and snowpacks with low scattering cross section at small and large solar zenith angles. Thirdly, changes of Q

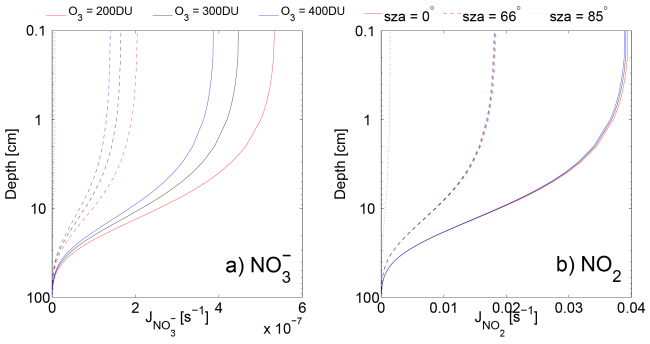

Figure 5. The effect of different column ozone amount on the photolysis rate coefficient of **(a)** NO_3^- and **(b)** NO_2 at three selected solar zenith angles (0°, 66° and 85°).

with increasing mass ratio of light-absorbing impurities depend on the chemical species being photolysed. All three of these effects depend on either the ratio of direct to diffuse radiation in the top of the snowpack or the conversion of direct solar radiation to diffuse solar radiation in the near-surface layer of the snowpack.

With regard to the density of the snowpack, the photolysis rate coefficient maxima are at a deeper depth for snowpacks with lower density. That is, the path length of the photon is longer for less-dense snowpacks. However, for the range of density values found in natural snow (case 1, $\rho = 0.2$–$0.6\,\mathrm{g\,cm^{-3}}$) the difference in the Q ratio is very small, of the order of $\sim 3.5\,\%$ (red symbols and lines in Fig. 3).

Scattering cross section of the snowpack: lower values of the scattering cross section imply longer path length of the photon between individual scattering events. Hence, the maximum photolysis rate coefficients tend to occur deeper into the snowpacks, as shown in blue in Fig. 6 (Scatt2, i.e. melting snow), compared with snowpacks that have a larger scattering cross section (magenta in Fig. 6, BaseC, i.e. cold polar snow). Thus for snowpacks with a small scattering cross section the agreement between the RT and z_e methods is likely to be poor as the z_e method will not capture the behaviour in the near-surface layer accurately.

Light-absorbing impurities in the snowpack: the propagation of actinic flux and the vertical variation of photolysis rate coefficient within snowpack is dominated by scattering when light-absorbing impurity contents are low and therefore the absorption properties of the impurity become unimportant, i.e. there is no difference between the value of Q for snowpack BC0.18 and HULIS1 listed in Table 3. In case 3, absorption due to black carbon, the variation of Q with solar zenith angle is approximately the same for the photolysis of NO_3^- ($\lambda \sim 321$ nm), H_2O_2($\lambda \sim 321$ nm), NO_2^- ($\lambda \sim 345$ nm) and NO_2($\lambda \sim 375$ nm). Except for heavily polluted snow, e.g. snowpack BC128 ($\rho = 0.4\,\mathrm{g\,cm^{-3}}$, $[\mathrm{BC}] = 128\,\mathrm{ng(C)\,g^{-1}}$ and $\sigma_{\mathrm{scatt}} = 25\,\mathrm{m^2\,kg^{-1}}$), the ratio Q for photolysis of the NO_2^- anion and NO_2 deviated from

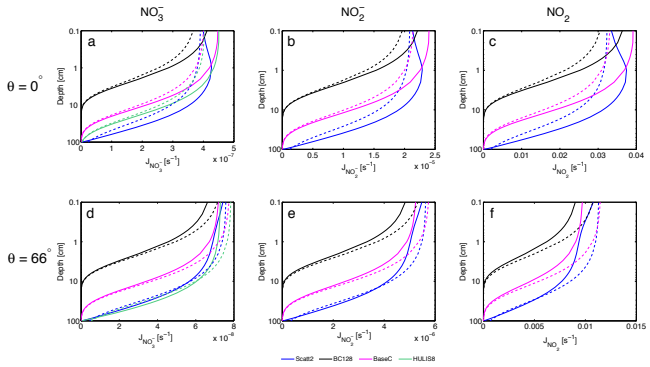

Figure 6. Photolysis rate coefficient for the NO_3^- anion (**a** and **d**), the NO_2^- anion (**b** and **e**) and NO_2 (**c** and **f**) computed by TUV (solid line) and z_e method (dashed line) at two different solar zenith angles, θ, at 0° (top row) and 66° (bottom row). Maximum and minimum depth-integrated photolysis rate coefficient ratio occurred at $\theta = 0°$ and $\theta = \sim 66°$ respectively. Blue is the "melting snow", Scatt2 ($\rho = 0.4\,\mathrm{g\,cm^{-3}}$, $[\mathrm{BC}] = 4\,\mathrm{ng(C)\,g^{-1}}$ and $\sigma_{\mathrm{scatt}} = 2\,\mathrm{m^2\,kg^{-1}}$); black is the "heavily black carbon polluted snow", BC128 ($\rho = 0.4\,\mathrm{g\,cm^{-3}}$, $[\mathrm{BC}] = 128\,\mathrm{ng(C)\,g^{-1}}$ and $\sigma_{\mathrm{scatt}} = 25\,\mathrm{m^2\,kg^{-1}}$); magenta is the "BaseC snow" BaseC ($\rho = 0.4\,\mathrm{g\,cm^{-3}}$, $[\mathrm{BC}] = 4\,\mathrm{ng(C)\,g^{-1}}$ and $\sigma_{\mathrm{scatt}} = 25\,\mathrm{m^2\,kg^{-1}}$); and green is the "HULIS-polluted snow", HULIS8 ($\rho = 0.4\,\mathrm{g\,cm^{-3}}$, $[\mathrm{HULIS}] = 8\,\mathrm{ng\,g^{-1}}$ and $\sigma_{\mathrm{scatt}} = 25\,\mathrm{m^2\,kg^{-1}}$). Surface (depth = 0 cm) values of photolysis rate coefficient from the "RT method" and "z_e method" are the same (see Eq. 8 for calculation of J_{TUV}).

snowpacks with lower black carbon mass ratio slightly (~ 3 and ~ 3.5 % respectively). In Fig. 6, black lines representing the extreme polluted case – BC128 – the photolysis rate coefficient calculated by the two methods matches at around 2 cm depth for the NO_3^- anion, but ~ 4 and ~ 5 cm for the NO_2^- and NO_2 respectively. The latter two compounds have the peak of their action spectrum at larger wavelengths relative to the NO_3^- anion and H_2O_2 as discussed in Sect. 3.2.2. The ratio of direct to diffuse incident solar radiation in the snowpack increases with wavelength around 300–400 nm and will increase the difference between the photolysis rate coefficient depth profile calculated by the z_e and RT methods especially in the top few centimetres of the snowpack.

In case 4, the absorption due to HULIS is considerable. A mass ratio of $100\,\mathrm{ng\,g^{-1}}$ of HULIS in the snowpack will reduce the photolysis of NO_3^- anion and H_2O_2 much more than the photolysis of NO_2^- and NO_2 as HULIS absorption cross section increases with decreasing wavelengths. The absorption cross section due to 1, 8, 17 and $1000\,\mathrm{ng\,g^{-1}}$ of HULIS is respectively equivalent to 0.18, 1.4, 3.0 and $177\,\mathrm{ng(C)\,g^{-1}}$ of black carbon at 321 nm, but only equivalent to 0.11, 0.87, 1.85 and $109\,\mathrm{ng(C)\,g^{-1}}$ of black carbon at 345 nm and 0.06, 0.50, 1.05 and $62.0\,\mathrm{ng(C)\,g^{-1}}$ of black carbon at 375 nm. If the light-absorption by impurities in a snowpack is dominated by black carbon, then the value of e-folding depth in the UV-B and UV-A will be similar. However, if the light-absorption in the snow is dominated by HULIS (or even dust), then strictly a different e-folding depth is needed for each wavelength that is characteristic of the photolysis of the species of interest.

Asymmetry factor of the snowpack: Libois et al. (2014) recently suggested that the value of the asymmetry parameter, g, should be $g = 0.86$ due to non-spherical grains observed in the laboratory and in the field in Antarctica and the French Alps. The e-folding depth is sensitive to the value of the asymmetry factor as shown by Libois et al. (2013). Reducing the asymmetry factor from 0.89 to 0.86 reduces the tendency of photons being forward-scattered, and hence the e-folding depth is reduced by ~ 11 %. The reduction in photolysis rate coefficient is also ~ 11 %. Nevertheless, there are no significant relative differences between the RT and z_e methods for changing g. The parameterisation with e-folding depth generated a similar approximation of photolysis rate coefficient for either of the two g values. The other properties of the snowpacks were unchanged.

3.3 Parameterisation correction

The difference in the depth-integrated photolysis rate coefficient, v, between the z_e method and RT method can be minimised by applying a correction factor, $C(\theta)$, as a function of the solar zenith angle. The correction factor, $C(\theta)$, was computed by fitting a quadratic equation to the plot of depth-integrated photolysis rate coefficient ratio, Q (Eq. 9), of each reaction as a function of solar zenith angle. The fitting is categorised into two types of snow – (1) wind pack and cold polar snow, and (2) melting and clean snow. Formulation of the correction factor, C, is shown in Eq. (10), and the coefficients (a, b, c) of the quadratic equation are listed in Tables 4 and 5 for "wind pack and cold polar" and "melting and clean" snow respectively. The depth-integrated photolysis rate coefficient approximated by the z_e method at a particular solar zenith angle can then be corrected by multiplying by the correction factor, $C(\theta)$, at that particular solar zenith angle as shown in Eq. (11).

$$C(\theta) = a\cos^2(\theta) + b\cos(\theta) + c, \tag{10}$$

$$v_{z_e}^{\mathrm{Corr}}(\theta) = C(\theta)v_{z_e}(\theta), \tag{11}$$

where $C(\theta)$ is the correction factor at a particular solar zenith angle; a, b, c are the coefficient of the quadric equation; v_{z_e} is the depth-integrated photolysis rate coefficients approximated by the z_e method; and $v_{z_e}^{\mathrm{Corr}}$ is the corrected depth-integrated photolysis rate coefficient v_{z_e}.

For snowpacks with a large e-folding depth, i.e. > 30 cm – for example either having a small scattering cross section or containing a small amount of light-absorbing impurities – it is suggested to apply correction factors for "melting and clean snow" when solar zenith angles are smaller than 50° and larger than 80° to reduce the error by 10–30 %. For snowpacks that have an e-folding depth smaller than 30 cm, the

Table 4. Parameterisation correction for "cold polar and coastal" snowpacks. Values of the correlation coefficient were calculated for two different snowpacks (BaseC, HULIS8 and Comb) with and without applying the correction factors.

				BaseC		HULIS8		Comb	
Species	a	b	c	R^2, v_{z_e}	$R^2, v_{z_e}^{\mathrm{Corr}}$	R^2, v_{z_e}	$R^2, v_{z_e}^{\mathrm{Corr}}$	R^2, v_{z_e}	$R^2, v_{z_e}^{\mathrm{Corr}}$
NO_3^-	0.452	−0.320	1.000	0.9788	0.9996	0.9862	0.9971	0.9468	0.9927
H_2O_2	0.485	−0.334	0.989	0.9758	0.9998				
NO_2^-	0.494	−0.345	0.980	0.9749	1.0000				
NO_2	0.758	−0.495	0.941	0.9435	0.9995				

Table 5. Parameterisation correction for "melting and clean" snowpack. Values of the correlation coefficient were calculated for two different snowpacks (Scatt2, HULIS1 and Comb) with and without applying the correction factors.

				Scatt2		HULIS1		Comb	
Species	a	b	c	R^2, v_{z_e}	$R^2, v_{z_e}^{\mathrm{Corr}}$	R^2, v_{z_e}	$R^2, v_{z_e}^{\mathrm{Corr}}$	R^2, v_{z_e}	$R^2, v_{z_e}^{\mathrm{Corr}}$
NO_3^-	0.523	−0.384	1.146	0.9004	0.9996	0.8742	0.9991	0.9481	0.9833
H_2O_2	0.550	−0.378	1.107	0.8503	0.9934				
NO_2^-	0.565	−0.394	1.106	0.8883	1.0000				
NO_2	0.868	−0.565	1.062	0.8352	0.9995				

"wind pack and cold polar snow" correction factors should be applied when the solar zenith angles are small than 30° or between 60 and 70°. This could reduce the error by up to 15 %.

The correction was evaluated by comparing the depth-integrated photolysis rate coefficients computed by the RT method, v_{TUV}, to depth-integrated photolysis rate coefficient approximated by the z_e method, v_{z_e}, and the corrected depth-integrated photolysis rate coefficient by the z_e method, $v_{z_e}^{\mathrm{Corr}}$, for all four species at 20 different solar zenith angles of snowpack BaseC (Table 3) using wind pack and cold polar snowpack correction factors, and results are shown in Fig. 7. For evaluating the melting and clean snowpack correction factors, snowpack Scatt2 (Table 3) was used, and results are shown in Fig. 8. The corrections factors for the NO_3^- photolysis rate coefficient were also tested against snowpacks HULIS1, HULIS8 and Comb (Table3).

The correlation between v_{z_e} and $v_{z_e}^{\mathrm{Corr}}$ with v_{TUV} is described by the square of correlation coefficients, R^2, listed in Tables 4 and 5 correction factors for wind pack and cold polar, and melting and clean snowpacks respectively. The approximation of depth-integrated photolysis rate coefficient has improved significantly with the correction factor, especially for (1) the melting and clean snowpack, (2) photolysis of the NO_2^- anion and (3) NO_2 at small solar zenith angles.

There are many factors that might have an impact on the disagreement between the two methods not taken into account in this study. Cloudy skies are not taken into account. However, clouds convert direct radiation into diffuse radiation. Under a very thickly clouded sky all radiation reaching the ground will be diffused and the decay of actinic flux within the snowpack would be exponential. Therefore, on a cloudy day the z_e method would provide a very good approximation of actinic flux profile and photolysis rate coefficient within snowpack even without correction. Other assumptions have also been made on snowpack properties, i.e. assuming homogeneous single-layer snowpack, black carbon or HULIS as the only absorber other than ice and constant vertical chemical concentration profile. Geographic location and weather conditions may have a major influence on the number of layers within snowpack and the distribution of their physical and optical properties. Last, but not least, field observations on the Antarctic Plateau (Frey et al., 2009; France et al., 2011) show there is a much higher nitrate anion concentration in the top few centimetres of the snowpack, the region of the snowpack where the solar radiation attenuation is often non-exponential, than deeper into the snowpack, causing a potentially larger error estimating depth-integrated production rates from the z_e method.

4 Conclusions

The parameterisation of snowpack actinic flux based on the e-folding depth – the z_e method, which approximates the actinic flux profile by an exponential function – may lead to under/overestimation of depth-integrated photolysis rate coefficients compared to the RT (radiative transfer) method. The deviation depends on the chemical species, solar zenith angle and properties of the snowpack. The z_e method is most likely to provide a poor estimation of depth-integrated photolysis rate under four conditions: (1) solar zenith angle or effective solar zenith angle being small (θ <37°); (2) the chemical species of interest having an action spectrum peak near or in the visible wavelength, such as NO_2^- and NO_2; (3) melting

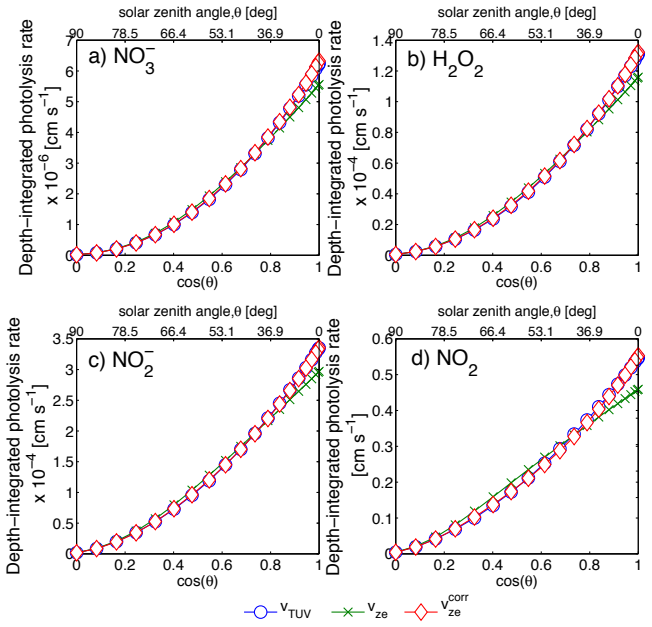

Figure 7. Depth-integrated photolysis rate coefficient at various solar zenith angle for different species within snowpack BaseC ($\rho = 0.4\,\mathrm{g\,cm^{-3}}$, $[\mathrm{BC}] = 4\,\mathrm{ng(C)\,g^{-1}}$ and $\sigma_{\mathrm{scatt}} = 25\,\mathrm{m^2\,kg^{-1}}$). **(a)** Depth-integrated photolysis rate coefficient of the NO_3^- anion; **(b)** depth-integrated photolysis rate coefficient of H_2O_2; **(c)** depth-integrated photolysis rate coefficient of the NO_2^- anion; **(d)** depth-integrated photolysis rate coefficient of NO_2; blue circle – v_{TUV}, computed by TUV; green cross – v_{z_e}, calculated by the e-folding depth method; pink diamond – $v_{z_e}^{\mathrm{Corr}}$, corrected v_{z_e} by coefficients listed in Table 4.

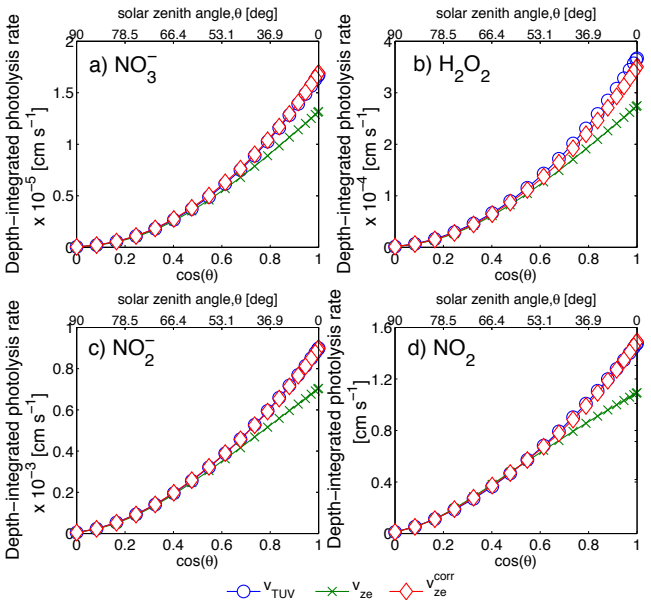

Figure 8. Depth-integrated photolysis rate coefficient at various solar zenith angle for different species within snowpack Scatt2 ($\rho = 0.4\,\mathrm{g\,cm^{-3}}$, $[\mathrm{BC}] = 4\,\mathrm{ng(C)\,g^{-1}}$ and $\sigma_{\mathrm{scatt}} = 2\,\mathrm{m^2\,kg^{-1}}$). **(a)** Depth-integrated photolysis rate coefficient of the NO_3^- anion; **(b)** depth-integrated photolysis rate coefficient of H_2O_2; **(c)** depth-integrated photolysis rate coefficient of the NO_2^- anion; **(d)** depth-integrated photolysis rate coefficient of NO_2; blue circle – v_{TUV}, computed by TUV; green cross – v_{z_e}, calculated by the e-folding depth method; red diamond – $v_{z_e}^{\mathrm{Corr}}$, corrected v_{z_e} by coefficients listed in Table 5.

snowpack, which has a small value of scattering cross section; and (4) clean snowpack, which has a small absorption cross section due to low impurity content.

The discrepancy between the z_e and RT methods can be improved by applying the correction factors, $C(\theta)$, especially for melting and clean snowpack (i.e. snowpacks have an e-folding depth larger than ∼30 cm), for which the ratio of depth-integrated photolysis rate coefficient between the two methods, Q, has reduced from 0.82–1.35 to 0.97–1.02 for photolysis of NO_2, from 0.88–1.28 to 0.99–1.02 for photolysis of the NO_2^- anion, from 0.93–1.27 to 0.99–1.03 for photolysis of the NO_3^- anion and from 0.91–1.28 to 0.98–1.06 for H_2O_2. In the polar regions, solar zenith angles larger than 42.8° are the norm; the simple z_e method provides an acceptable estimation (10–16 % underestimation compared to radiative transfer model). However, if the site of interest is a tropical glacier, low-latitude, slope snowpack or have a small effective solar zenith angle ($\theta < 37°$) and is moderately to heavily polluted (e.g. e-folding depth smaller than 30 cm), then correction factors, C, from Tables 4 should be applied to reduce error up to 15 %. Correction factors, C, listed in Table 5 should be applied when the snowpack is clean, wet or melting (e.g. e-folding depth larger than 31 cm) to reduce the difference by up to 30 %.

The values of e-folding depth used in some of the previous modelling studies were broadly based on field measurements (Thomas et al., 2011; Simpson et al., 2002). Recently research groups have started to develop new algorithms to estimate optical properties of snowpack, such as grain size and mass ratio of pollutants, from satellite measurements (Zege et al., 2011; Malinka, 2014; Khokanovsky, 2015). These measurements and algorithms can be integrated into large-scale chemical transport models in the future to estimate e-folding depth and photolysis rate coefficient for wide inaccessible areas.

An important approximation of the e-folding depth (z_e) method is that snowpack is optically thick, i.e. assuming the snowpacks are semi-infinite. For shallow snowpacks the exact RT method should be used. It is unlikely a robust simple parameterisation could be developed to correct the z_e method for shallow snowpacks over a range of light-absorbing snowpack, solar zenith angles and underlying terrains for the thin snowpack, i.e. soil or sea ice. For shallow snowpacks (< 2–3 e-folding depths) the RT method is recommended.

Appendix A

Table A1. Notation.

σ	Absorption cross section of chemical species	$cm^2\,molecule^{-1}$
σ_{ice}	Absorption cross section of ice	$cm^2\,kg^{-1}$
μ_{abs}	Absorption coefficient	m^{-1}
σ^+	Absorption cross section per mass of impurities	$cm^2\,kg^{-1}$
I	Actinic flux	$quanta\,cm^{-2}\,s^{-1}\,nm^{-1}$
z_e	Asymptotic e-folding depth	cm
g	Asymmetry factor	dimensionless
c	Correction factor for depth-integrated photolysis rate coefficient	dimensionless
ρ	Density of snowpack	$g\,cm^{-3}$
κ_{ext}	Extinction coefficient	m^{-1}
σ_{ext}	Extinction cross section	$m^2\,kg^{-1}$
J	Photolysis rate constant	s^{-1}
F	Photochemical production rate	$\mu mol\,cm^{-2}\,s^{-1}$
Φ	Quantum yield	dimensionless
Q	Quotient, ratio of depth-integrated photolysis rate coefficient	dimensionless
r_{scatt}	Scattering coefficient	m^{-1}
σ_{scatt}	Scattering cross section	$m^2\,kg^{-1}$
θ	Solar zenith angle	degree
σ_{abs}	Total absorption cross section	$cm^2\,kg^{-1}$
v	depth-integrated photolysis rate coefficient	$cm\,s^{-1}$
λ	Wavelength	nm

Acknowledgements. H. G. Chan is funded by the Natural Environment Research Council through Doctoral Studentship NE/L501633/1.

Edited by: T. Bartels-Rausch

References

Anastasio, C. and Chuand, L.: Formation of hydroxyl radical from the photolysis of frozen hydrogen peroxide, J. Phys. Chem. A, 112, 2747–2748, doi:10.1021/jp800491n, 2008.

Bartels-Rausch, T., Jacobi, H.-W., Kahan, T. F., Thomas, J. L., Thomson, E. S., Abbatt, J. P. D., Ammann, M., Blackford, J. R., Bluhm, H., Boxe, C., Domine, F., Frey, M. M., Gladich, I., Guzmán, M. I., Heger, D., Huthwelker, Th., Klán, P., Kuhs, W. F., Kuo, M. H., Maus, S., Moussa, S. G., McNeill, V. F., Newberg, J. T., Pettersson, J. B. C., Roeselová, M., and Sodeau, J. R.: A review of air-ice chemical and physical interactions (AICI): liquids, quasi-liquids, and solids in snow, Atmos. Chem. Phys., 14, 1587–1633, doi:10.5194/acp-14-1587-2014, 2014.

Beaglehole, D., Ramanathan, B., and Rumberg, J.: The UV to IR transmittance of Antarctic snow, J. Geophys. Res.-Atmos., 103, 8849–8857, doi:10.1029/97JD03604, 1998.

Beine, H. J., Dominé, F., Simpson, W., Honrath, R. E., Sparapani, R., Zhou, X., and King, M.: Snow-pile and chamber experiments during the Polar Sunrise Experiment "Alert 2000": exploration of nitrogen chemistry, Atmos. Environ., 36, 2707–2719, doi:10.1016/S1352-2310(02)00120-6, 2002.

Beine, H. J., Amoroso, A., Dominé, F., King, M. D., Nardino, M., Ianniello, A., and France, J. L.: Surprisingly small HONO emissions from snow surfaces at Browning Pass, Antarctica, Atmos. Chem. Phys., 6, 2569–2580, doi:10.5194/acp-6-2569-2006, 2006.

Chen, G., Davis, D., Crawford, J., Hutterli, L., Huey, L., Slusher, D., Mauldin, L., Eisele, F., Tanner, D., Dibb, J., Buhr, M., McConnell, J., Lefer, B., Shetter, R., Blake, D., Song, C., Lombardi, K., and Arnoldy, J.: A reassessment of HO_x South Pole chemistry based on observations recorded during ISCAT 2000, Atmos. Environ., 38, 5451–5461, 2004.

Chu, L. and Anastasio, C.: Quantum yields of hydroxyl radical and nitrogen dioxide from the photolysis of nitrate on ice, J. Phys. Chem. A, 107, 9594–9602, doi:10.1021/jp0349132, 2003.

Chu, L. and Anastasio, C.: Formation of hydroxyl radical from the photolysis of frozen hydrogen peroxide, J. Phys. Chem. A, 109, 6264–6271, doi:10.1021/jp051415f, 2005.

Chu, L., and Anastasio, C.: Temperature and wavelength dependence of nitrite photolysis in frozen and aqueous solutions, Environ. Sci. Technol., 41, 3626–3632, doi:10.1021/es062731q, 2007.

Cotter, E. S. N., Jones, A. E., Wolff, E. W., and Bauguitte, S. J.-B.: What controls photochemical NO and NO_2 production from Antarctic snow? Laboratory investigation assessing the wavelength and temperature dependence, J. Geophys. Res.-Atmos., 108, 4147 , doi:10.1029/2002JD002602, 2003.

Davis, D., Chen, G., Buhr, M., Crawford, J., Lenschow, D., Lefer, B., Shetter, R., Eisele, F., Mauldin, L., and Hogan, A.: South Pole chemistry: an assessment of factors controlling variability and absolute levels, Atmos. Environ., 38, 5375–5388, 2004.

DeMore, W. B., C. J. Howard, D. M. G., Kolb, C. E., Hampson, R. F., and Molina, M. J.: Chemical Kinetics and Photochemical Data for Use in Stratospheric Modeling, JPL Publication 97–4, National Aeronautics and Space Administration, Jet Propulsion Laboratory, Pasadena, California, USA, 1997.

Dibb, J. E., Arsenault, M., Peterson, M. C., and Honrath, R. E.: Fast nitrogen oxide photochemistry in Summit, Greenland snow, Atmos. Environ., 36, 2501–2511, 2002.

Dubowski, Y., Colussi, A. J., and Hoffmann, M. R.: Nitrogen dioxide release in the 302 nm band photolysis of spray-frozen aqueous nitrate solutions. Atmospheric implications, J. Phys. Chem. A, 105, 4928–4932, doi:10.1021/jp0042009, 2001.

Dubowski, Y., Colussi, A. J., Boxe, C., and Hoffmann, M. R.: Monotonic increase of nitrite yields in the photolysis of nitrate in ice and water between 238 and 294 K, J. Phys. Chem. A, 106, 6967–6971, doi:10.1021/jp0142942, 2002.

Fisher, F. N., King, M. D., and Lee-Taylor, J.: Extinction of UV-visible radiation in wet midlatitude (maritime) snow: implications for increased NO_x emission, J. Geophys. Res.-Atmos., 110, D21301, doi:10.1029/2005JD005963, 2005.

France, J. and King, M.: The effect of measurement geometry on recording solar radiation attenuation in snowpack (*e*-folding depth) using fibre-optic probes, J. Glaciol., 58, 417–418, doi:10.3189/2012JoG11J227, 2012.

France, J., King, M., and Lee-Taylor, J.: Hydroxyl (OH) radical production rates in snowpacks from photolysis of hydrogen peroxide (H_2O_2) and nitrate (NO_3^-), Atmos. Environ., 41, 5502–5509, doi:10.1016/j.atmosenv.2007.03.056, 2007.

France, J., King, M., and Lee-Taylor, J.: The importance of considering depth-resolved photochemistry in snow: a radiative-transfer study of NO_2 and OH production in Ny-alesund (Svalbard) snowpacks, J. Glaciol., 56, 655–663, doi:10.3189/002214310793146250, 2010.

France, J. L., King, M. D., Frey, M. M., Erbland, J., Picard, G., Preunkert, S., MacArthur, A., and Savarino, J.: Snow optical properties at Dome C (Concordia), Antarctica; implications for snow emissions and snow chemistry of reactive nitrogen, Atmos. Chem. Phys., 11, 9787–9801, doi:10.5194/acp-11-9787-2011, 2011.

France, J. L., Reay, H. J., King, M. D., Voisin, D., Jacobi, H. W., Domine, F., Beine, H., Anastasio, C., MacArthur, A., and Lee-Taylor, J.: Hydroxyl radical and NO_x production rates, black carbon concentrations and light-absorbing impurities in snow from field measurements of light penetration and nadir reflectivity of onshore and offshore coastal Alaskan snow, J. Geophys. Res.-Atmos., 117, D00R12, doi:10.1029/2011JD016639, 2012.

Frey, M. M., Savarino, J., Morin, S., Erbland, J., and Martins, J. M. F.: Photolysis imprint in the nitrate stable isotope signal in snow and atmosphere of East Antarctica and implications for reactive nitrogen cycling, Atmos. Chem. Phys., 9, 8681–8696, doi:10.5194/acp-9-8681-2009, 2009.

Gardner, E. P., Sperry, P. D., and Calvert, J. G.: Primary quantum yields of NO_2 photodissociation, J. Geophys. Res.-Atmos., 92, 6642–6652, doi:10.1029/JD092iD06p06642, 1987.

Grannas, A. M., Jones, A. E., Dibb, J., Ammann, M., Anastasio, C., Beine, H. J., Bergin, M., Bottenheim, J., Boxe, C. S., Carver, G., Chen, G., Crawford, J. H., Dominé, F., Frey, M. M., Guzmán,

M. I., Heard, D. E., Helmig, D., Hoffmann, M. R., Honrath, R. E., Huey, L. G., Hutterli, M., Jacobi, H. W., Klán, P., Lefer, B., McConnell, J., Plane, J., Sander, R., Savarino, J., Shepson, P. B., Simpson, W. R., Sodeau, J. R., von Glasow, R., Weller, R., Wolff, E. W., and Zhu, T.: An overview of snow photochemistry: evidence, mechanisms and impacts, Atmos. Chem. Phys., 7, 4329–4373, doi:10.5194/acp-7-4329-2007, 2007.

Grenfell, T. C., Warren, S. G., and Mullen, P. C.: Reflection of solar radiation by the Antarctic snow surface at ultraviolet, visible, and near-infrared wavelengths, J. Geophys. Res.-Atmos., 99, 18669–18684, doi:10.1029/94JD01484, 1994.

Hoffer, A., Gelencsér, A., Guyon, P., Kiss, G., Schmid, O., Frank, G. P., Artaxo, P., and Andreae, M. O.: Optical properties of humic-like substances (HULIS) in biomass-burning aerosols, Atmos. Chem. Phys., 6, 3563–3570, doi:10.5194/acp-6-3563-2006, 2006.

Jacobi, H.-W., Bales, R. C., Honrath, R. E., Peterson, M. C., Dibb, J. E., Swanson, A. L., and Albert, M. R.: Reactive trace gases measured in the interstitial air of surface snow at Summit, Greenland, Atmos. Environ., 38, 1687–1697, doi:10.1016/j.atmosenv.2004.01.004,2004.

Jones, A. E., Weller, R., Wolff, E. W., and Jacobi, H. W.: Speciation and rate of photochemical NO and NO_2 production in Antarctic snow, Geophys. Res. Lett., 27, 345–348, doi:10.1029/1999GL010885, 2000.

Khokanovsky, A. A.: Remote Sensing of the Cryosphere, Ch4 Remote sensing of snow albedo, grain size, and pollution from space, 48–72, John Wiley & Sons, Ltd, Chichester, UK, doi:10.1002/9781118368909.ch4, 2015.

King, M. D. and Simpson, W. R.: Extinction of UV radiation in Arctic snow at Alert, Canada (82° N), J. Geophys. Res.-Atmos., 106, 12499–12507, doi:10.1029/2001JD900006, 2001.

Kroon, M., Veefkind, J. P., Sneep, M., McPeters, R. D., Bhartia, P. K., and Levelt, P. F.: Comparing OMI-TOMS and OMI-DOAS total ozone column data, J. Geophys. Res.-Atmos., 113, D16S28, doi:10.1029/2007JD008798, 2008.

Kramarova, N. A., Nash, E. R., Newman, P. A., Bhartia, P. K., McPeters, R. D., Rault, D. F., Seftor, C. J., Xu, P. Q., and Labow, G. J.: Measuring the Antarctic ozone hole with the new Ozone Mapping and Profiler Suite (OMPS), Atmos. Chem. Phys., 14, 2353–2361, doi:10.5194/acp-14-2353-2014, 2014.

Lee-Taylor, J. and Madronich, S.: Calculation of actinic fluxes with a coupled atmosphere–snow radiative transfer model, J. Geophys. Res., 107, 4796, doi:10.1029/2002JD002084, 2002.

Libois, Q., Picard, G., France, J. L., Arnaud, L., Dumont, M., Carmagnola, C. M., and King, M. D.: Influence of grain shape on light penetration in snow, The Cryosphere, 7, 1803–1818, doi:10.5194/tc-7-1803-2013, 2013.

Libois, Q., Picard, G., Dumont, M., Arnaud, L., Sergent, C., Pougatch, E., Sudul, M., and Vial, D.: Experimental determination of the absorption enhancement parameter of snow, J. Glaciol., 60, 714–724, 2014.

Malinka, A. V.: Light scattering in porous materials: Geometrical optics and stereological approach, J. Quant. Spectrosc. Radiat. Transfer, 141, 14–23, doi:http://dx.doi.org/10.1016/j.jqsrt.2014.02.022, 2014.

Marks, A. A. and King, M. D.: The effect of snow/sea ice type on the response of albedo and light penetration depth (*e*-folding depth) to increasing black carbon, The Cryosphere, 8, 1625–1638, doi:10.5194/tc-8-1625-2014, 2014.

Mauldin, R. L., Eisele, F. L., Tanner, D. J., Kosciuch, E., Shetter, R., Lefer, B., Hall, S. R., Nowak, J. B., Buhr, M., Chen, G., Wang, P., and Davis, D.: Measurements of OH, H_2SO_4, and MSA at the South Pole during ISCAT, Geophys. Res. Lett., 28, 3629–3632, doi:10.1029/2000GL012711, 2001.

McNeill, V. F., Grannas, A. M., Abbatt, J. P. D., Ammann, M., Ariya, P., Bartels-Rausch, T., Domine, F., Donaldson, D. J., Guzman, M. I., Heger, D., Kahan, T. F., Klán, P., Masclin, S., Toubin, C., and Voisin, D.: Organics in environmental ices: sources, chemistry, and impacts, Atmos. Chem. Phys., 12, 9653–9678, doi:10.5194/acp-12-9653-2012, 2012.

Simpson, W. R., King, M. D., Beine, H. J., Honrath, R. E., and Zhou, X.: Radiation-transfer modeling of snow-pack photochemical processes during ALERT 2000, Atmos. Environ., 36, 2663–2670, doi:10.1016/S1352-2310(02)00124-3, 2002.

Sjostedt, S. J., Huey, L. G., Tanner, D. J., Peischl, J., Chen, G., Dibb, J. E., Lefer, B., Hutterli, M. A., Beyersdorf, A. J., Blake, N. J., and Blake, D. R.: Peroxy and hydroxyl radical measurements during the spring 2004 Summit Field Campaign, American Geophysical Union, Fall Meeting 2005, abstract #A24A-02, 2005AGUFM.A24A..02S, 5–9 December 2005, San Francisco, CA, USA, 2005.

Thomas, J. L., Stutz, J., Lefer, B., Huey, L. G., Toyota, K., Dibb, J. E., and von Glasow, R.: Modeling chemistry in and above snow at Summit, Greenland – Part 1: Model description and results, Atmos. Chem. Phys., 11, 4899–4914, doi:10.5194/acp-11-4899-2011, 2011.

Voisin, D., Jaffrezo, J.-L., Houdier, S., Barret, M., Cozic, J., King, M. D., France, J. L., Reay, H. J., Grannas, A., Kos, G., Ariya, P. A., Beine, H. J., and Domine, F.: Carbonaceous species and humic like substances (HULIS) in Arctic snowpack during OASIS field campaign in Barrow, J. Geophys. Res.-Atmos., 117, D00R19, doi:10.1029/2011JD016612, 2012.

Warneck, P. and Wurzinger, C.: Product quantum yields for the 305-nm photodecomposition of nitrate in aqueous solution, J. Phys. Chem., 92, 6278–6283, doi:10.1021/j100333a022, 1988.

Warren, S. G.: Optical properties of snow, Rev. Geophys., 20, 67–89, doi:10.1029/RG020i001p00067, 1982.

Warren, S. G. and Brandt, R. E.: Optical constants of ice from the ultraviolet to the microwave: a revised compilation, J. Geophys. Res.-Atmos., 113, D14220, doi:10.1029/2007JD009744, 2008.

Warren, S. G. and Wiscombe, W. J.: A model for the spectral albedo of snow. II: Snow containing atmospheric aerosols, J. Atmos. Sci., 37, 2734–2745, doi:10.1175/1520-0469(1980), 1980.

Warren, S. G., Brandt, R. E., and Grenfell, T. C.: Visible and near-ultraviolet absorption spectrum of ice from transmission of solar radiation into snow, Appl. Optics, 45, 5320–5334, doi:10.1364/AO.45.005320, 2006.

Wiscombe, W. J. and Warren, S. G.: A model for the spectral albedo of snow. I: Pure snow, J. Atmos. Sci., 37, 2712–2733, doi:10.1175/1520-0469(1980)037<2712:AMFTSA>2.0.CO;2, 1980.

Wolff, E. W. and Bales, R. C.: Chemical Exchange Between the Atmosphere and Polar Snow, NATO ASI Series, 43, Springer, Berlin, Heidelberg, Germany, 1996.

Zatko, M. C., Grenfell, T. C., Alexander, B., Doherty, S. J., Thomas, J. L., and Yang, X.: The influence of snow grain size and im-

purities on the vertical profiles of actinic flux and associated NO_x emissions on the Antarctic and Greenland ice sheets, Atmos. Chem. Phys., 13, 3547–3567, doi:10.5194/acp-13-3547-2013, 2013.

Zege, E. P., Katsev, I. L., Malinka, A. V., Prikhach, A. S., Heygster, G., and Wiebe, H.: Algorithm for retrieval of the effective snow grain size and pollution amount from satellite measurements, Remote Sens. Environ., 115, 2674–2685, doi:10.1016/j.rse.2011.06.001, 2011.